Solid Freeform Fabrication 2023: Proceedings of the 34th Annual International Solid Freeform Fabrication Symposium – An Additive Manufacturing Conference
Reviewed Paper

Analytical Modeling of Cooling Rates in PBF-LB/M of Bulk Metallic Glasses

Hanna Schönrath[1] *, Jan Wegner[1], Maximilian Frey[2], Erika Soares Barreto[3], Arno Elspaß[1], Norman Schnell[1], Benjamin H. R. Erdmann[1], Julian Neises[4], Nils Ellendt[3], Ralf Busch[2], Stefan Kleszczynski[1,5]

[1]Chair of Manufacturing Technology, University of Duisburg-Essen, Lotharstraße 1, 47057 Duisburg, Germany
[2]Chair of Metallic Materials, Saarland University, Campus C6.3, 66123 Saarbrücken, Germany
[3] Leibniz Institute for Materials Engineering—IWT, Badgasteiner Str. 3, 28359 Bremen, Germany
[4] Institute of Technology for Nanostructures, University Duisburg-Essen, 47057 Duisburg, Germany.
[5]Center for Nanointegration Duisburg-Essen (CENIDE), Carl-Benz-Str. 199, 47057 Duisburg, Germany

*corresponding author
hanna.schoenrath@uni-due.de
Tel.: + 49 203 / 379 1181
Fax.: + 49 231 / 379 1530

Abstract

Additive manufacturing through laser powder bed fusion (PBF-LB/M) inheres great potential for the processing of bulk metallic glasses (BMGs). The size-independent high cooling rates during the process benefit the fabrication of large and elaborate amorphous components. Albeit, partial crystallization poses a challenge in additively manufactured BMGs, potentially limiting the resulting mechanical properties. In this matter, the complex thermal history during processing often states a remaining uncertainty. Besides in situ measurements and numerical estimations, analytical models can be used to achieve a deeper understanding of the transient temperature evolution. In this work, an iterative solution to the analytical Rosenthal equation is developed and applied to ZrCuAlNb- and CuTiZrNi-BMGs to predict melt pool dimensions and cooling rates during PBF-LB/M. Therefore, temperature-dependent thermal properties are determined via laser flash measurements. The effective absorptivity of the two materials is measured, and single-line experiments were performed as a validation for the approach.

Keywords: Bulk Metallic Glasses, Additive Manufacturing, PBF-LB/M, Rosenthal Model

Introduction

Additive manufacturing (AM) is widely recognized for its high design freedom, individualization capabilities, and lightweight design. Recently possibilities to manufacture novel advanced materials are brought into focus. Among the various AM technologies, laser powder bed fusion (PBF-L/BM) has reached a significant level of technological maturity for metallic parts. The experience with standard materials is high, and applications on an industrial scale are already being implemented [1]. However, the exploration of new materials that can

fully benefit from the specific process characteristics – i.e., layer-wise buildup, high heating and cooling rates – is still subject to research. One promising alloy class for the processing via PBF-LB/M is the bulk metallic glasses (BMGs) [2, 3]. These materials exhibit higher strength, elasticity, and superior cryogenic properties compared to crystalline alloys [4]. The emergence of an amorphous structure in a metallic alloy requires rapid cooling with an alloy specific so called critical cooling rate (R_{crit}).

In conventional processing routes, these rates are typically difficult to achieve with increasing volume to surface ratio, which effectively limits the manufacturable size of BMGs to several millimeters [5]. In contrast, PBF-LB/M inherently features high cooling rates of 10^6 to 10^7 K/s [6], which exceeds the R_{crit} of most BMGs by several orders of magnitude. This theoretically enables the manufacturing of large and complex BMGs. Nevertheless, in practical applications, partial crystallization is frequently observed [7–13]. The layer-wise deposition of powder and vector-based heating implies a heat treatment of the surrounding solidified material. Additionally, contaminations of atomized powders and the influence of the process gas are considered to affect the structure of fabricated materials [14, 15]. Consequently, to ascertain vitrification despite the uncertain limitations, alloys with comparatively high glass-forming ability (GFA) are preferably chosen.

Despite the potential of PBF-LB/M, the reported high cooling rates suggest that its capabilities have not been fully exploited yet. The mechanism underlying crystallization and vitrification is not yet fully understood, and experimental determination of the complex thermal cycling during additive manufacturing processes on a meso scale cannot easily be performed. Analytical methods for determining cooling rates and melt pool dimensions could enable an estimation of the processability, including vitrification of novel material classes with lower GFA. Further, the choice of adequate process parameters could be based on the analytically determined viable cooling rates and melt pool dimensions, enabling an accelerated investigation of novel and processable BMGs.

Analytical Rosenthal model

An analytical approach to describe the heat dissipation during laser welding was developed by Rosenthal in [16] (eq. 1). It is based on a moving point heat source as energy input, constant material parameters, and conduction as the only heat loss:

$$T = T_0 + \frac{aP_L}{2\pi k\delta} \cdot e^{-\frac{v_s\,(\delta+\xi)}{2\tau}} \qquad \text{Eq. 1}$$

with the coordinates x (in scanning direction), y (width of scan track), and z (depth of the melt pool); T_0 = temperature of surroundings, T = temperature at a specific point (x|y|z), a = absorptivity, P_L= laser power, k = thermal conductivity, v_s = speed of heat source (moves along x), τ = thermal diffusivity, $\xi = x - v_s \cdot t$ is the distance of point (x|y|z) to heat source in x direction. $\delta = \sqrt{\xi^2 + y^2 + z^2}$ is the radial distance of point (x|y|z) to the heat source.

Despite the simplifications, several studies demonstrated the viability of the Rosenthal model to approximate the temperature distribution during PBF-LB/M [17–19]. For instance, Promoppattum et al. used the Rosenthal equation to predict the dendrite spacing of IN718 in [17]. In PBF-LB/M the main heat transfer mechanism changes with increasing energy input from conduction mode (dissipation into surrounding solid material) to keyhole mode (evaporation and plasma) [20]. One can conclude that the validity of the model is higher for

processing parameters in conduction mode. Since crystallization needs to be avoided in processing BMGs, low energy densities are typically preferred [13, 21]. Consequently, keyhole mode is generally avoided in BMG processing [22], and the Rosenthal equation potentially allows meaningful estimations for the apparent temperature profiles. Additionally, latent heat and phase transitions are presumably irrelevant during vitrification, further enhancing the practicality of the approach. However, there are remaining uncertainties regarding the assumption of constant thermophysical properties and the unknown absorptivity. Metallic materials typically feature large temperature dependencies of their thermal conductivity and diffusivity. It is reasonable to assume that BMGs also display similar temperature dependencies, which should be taken into consideration when applying the analytical model.

This work targets the analytical description of the melt pool dimensions and cooling rates during PBF-LB/M of BMGs based on the Rosenthal model. Thereby a fundamental understanding of the time-temperature regime present during the laser material interaction is established. Temperature dependencies of the thermal conductivity and diffusivity are determined and inserted into the Rosenthal equation. Two glass-forming alloys, $Zr_{59.3}Cu_{28.8}Al_{10.4}Nb_{1.5}$ (AMZ4, trade name: Zr0) and $Cu_{47}Ti_{34}Zr_{11}Ni_8$ (Vit101) are chosen for the analysis. AMZ4 is a commercially available glass forming alloy, whereas Vit101 is known and investigated, but not yet commercialized. They inhere outstanding material properties, such as an elasticity exceeding conventional materials by ~2%, combined with a flexural strength of 2.1 GPa and 2.5 GPa. The selection of these materials allows for a comparison between analytically predicted and experimentally determined melt pool widths, aiming to validate the model. The novel glass-forming alloy $Ti_{60}Zr_{15}Cu_{17}S_8$ (Ti60S) is a prospect for PBF-LB/M with an extraordinary yield strength of ~3 GPa, exceeding conventionally manufactured Ti6Al4V by 200%. Additionally, biocompatibility and corrosion resistance are favoring this material. The feasibility study concerning manufacturing amorphous $Ti_{60}Zr_{15}Cu_{17}S_8$ single tracks by PBF-LB/M completes this work.

Materials and Methods

BMG Alloys

For the three chosen glass-forming alloys AMZ4, Vit101, and $Ti_{60}Zr_{15}Cu_{17}S_8$,the physical properties are given in Tab. 1. Gas atomized powder feedstock was used for the processing of single lines of AMZ4 and Vit101.

As a measure for the GFA, the critical diameter D_c [cm], the highest possible diameter at which the whole structure solidifies amorphous during casting, is present. Based on this, the critical cooling rate in K/s [23] is:

$$R_{crit} = \frac{10}{(D_c)^2} \qquad \text{Eq. 2}$$

This is used as a reference value for the comparison to the calculated cooling rates in additive manufacturing:

$$R = \frac{T_l - T_g}{t_c} \qquad \text{Eq. 3}$$

Table 1: Composition and physical properties of selected glass-forming materials.

Physical property	**AMZ4**	**Vit101**	**Ti60S ([24])**
Composition [at%]	$Zr_{59.3}Cu_{28.8}Al_{10.4}Nb_{1.5}$	$Cu_{47}Ti_{34}Zr_{11}Ni_8$	$Ti_{60}Zr_{15}Cu_{17}S_8$
Density	6.68 g/cm³ [147]	6.89 g/cm³ [25]	5.5 g/cm³
Liquidus temperature T_l	1193 K [26]	1168 K [25]	1365 K
Solidus temperature T_s	1143 K [27]	1067 K [25]	-
Glass transition temperature T_g	671 K [26]	690 K [25]	675 K
Crystallization temperature T_x	748 K [26]	710 K [25]	752 K
Critical casting diameter D_C	5-14 mm [28]	4-5 mm [23, 25]	1 mm
Critical cooling rate R_{crit} (acc. to eq. 2)	5 - 40 K/s	20 - 62 K/s	1000 K/s

Sample analysis

The thermal conductivity was measured by the laser flash method. Measurements were performed with a NETZSCH LFA 457 MicroFlash to assess the temperature-dependent thermal conductivity by measuring the thermal diffusivity [29]. Vit101 samples, in the form of pellets, possess a diameter of approximately 10 mm and a thickness of 3 mm. They were coated with graphite on both surfaces to improve their absorption/emission characteristic. The measurements were carried out in an argon atmosphere (purge flow of 75 ml/min) within a temperature range from room temperature to 1073 K, in temperature steps of 100 K. Additional measurement steps were chosen at 623, 723, and 753 K to cover the phase change. Each sample was measured twice. Stepwise heating with 0.02 K/s and holding periods of ~280 s is applied. The specific heat capacity was determined using an equation proposed by Kubaschewski [30] and fitting parameters by Bochtler [25], assuming a crystalline material behavior. The thermal conductivity was calculated employing the procedure introduced by Parker et al. [31] using an improved Cape-Lehman model [32] within the analysis software provided by the LFA manufacturer (NETZSCH LFA Analysis version 7.1.0).

Finally, the absorptivity is required for the Rosenthal equation. The energy absorption during the laser material interaction in PBF-LB/M has been extensively discussed in the literature over the last decade. One uncertainty is the coexistence of bulk, powder, liquid, and plasma within the interaction zone. This renders conventional techniques such as measurements with an Ulbrich-sphere challenging during the process. Attempts for ray-tracing simulations [33] and analytical calculations based on Hagen-Rubens [34] typically neglect the impact of fume and gas flow during the PBF-LB/M process. Results from Ye et al. imply that the liquid melt is the main absorbing medium. However, obtaining the necessary physical properties of liquid metallic melts for analytical or numerical calculations are difficult to obtain and rarely reported. An alternative approach to determine the energy coupling during PBF-LB/M is the calorimetric determination as initially presented by Trapp and adapted by Schnell et al. in [35] and [36]. This setup is used to determine the effective absorptivity of AMZ4 and Vit101. The

absorptivity of $Ti_{60}Zr_{15}Cu_{17}S_8$ is determined by the application of eq. 4 which is derived from the Rosenthal equation (eq. 1):

$$a \approx \frac{2D^2 * \rho \cdot C_p \cdot v \cdot (T_l - T_0) * \pi e}{8 * P} \qquad \text{Eq. 4}$$

where 2D is the weld track width of single tracks, processed in a PBF-LB/M machine on cast material, due to the lack of atomized powder in this feasibility study.

PBF-LB/M processing

For empirical validation, single lines are processed via PBF-LB/M. For the sake of comparison and transferability of the results, two alloys and different manufacturing systems are applied. Argon atomized powder of the BMG-forming alloy $Cu_{47}Ti_{34}Zr_{11}Ni_8$ (in -at.%), with a particle size of 20-63 µm (here called: Vit101), described in detail in [15], and commercially available Zr0 from Heraeus AMLOY Technology (here called by its former name: AMZ4) are used for this study. PBF-LB/M experiments on Vit101 are carried out using the SLM 280 HL system from SLM Solutions, equipped with a 700 W fiber laser and a nominal spot size of 70 µm. Samples are processed with a layer thickness ds = 20 µm and, if applicable, hatch *h* of 90 µm. AMZ4 is processed on an M100 eos with a nominal laser spot diameter of 40 µm and a maximal laser power output of 200 W. The experiments are conducted in Argon atmosphere (Arcal Prime, 99.998 vol.%). The individual parameters are listed in Tab. A-2 in the appendix. The line energy density E_L according to Meiners is used as equivalent for the energy input at different parameter combinations according to eq. 5 [37]:

$$E_L = \frac{P}{v} \qquad \text{Eq. 5}$$

Results and discussion

Thermophysical properties

As an essential input variable for the Rosenthal equation (see eq 1.), the thermal conductivity of the investigated alloys is analyzed initially. Fig. 1 illustrates the thermal diffusivity τ plotted over the temperature from 293 K to 1073 K of the initially amorphous samples (run 1) and the partially crystallized sample (run 2). The thermal conductivity is shown in Fig. 2 respectively. Additionally, the coefficients described by Lindwall [38] are depicted for AMZ4 as a reference.

Values of the amorphous samples increase steadily starting from $k_{295,4\,K}^{Vit101}$= 5.17 W/(mK) and $k_{295,4\,K}^{AMZ4}$= 5.7 W/(mK) until the temperature reaches 674 K. Here, the discontinuous rise of the coefficient can be associated with the glass transition and crystallization of the samples. The values roughly match T_g of each respective material. During the second heating procedure, a continuous progress of the thermal conductivity indicates the absence of a phase transition, thus implying a crystallized sample. The distinct difference in the heat conductivity between the amorphous and crystalline phase agrees with the result of Yamasaki et al. and originates from the highly alloyed solid solution [39].

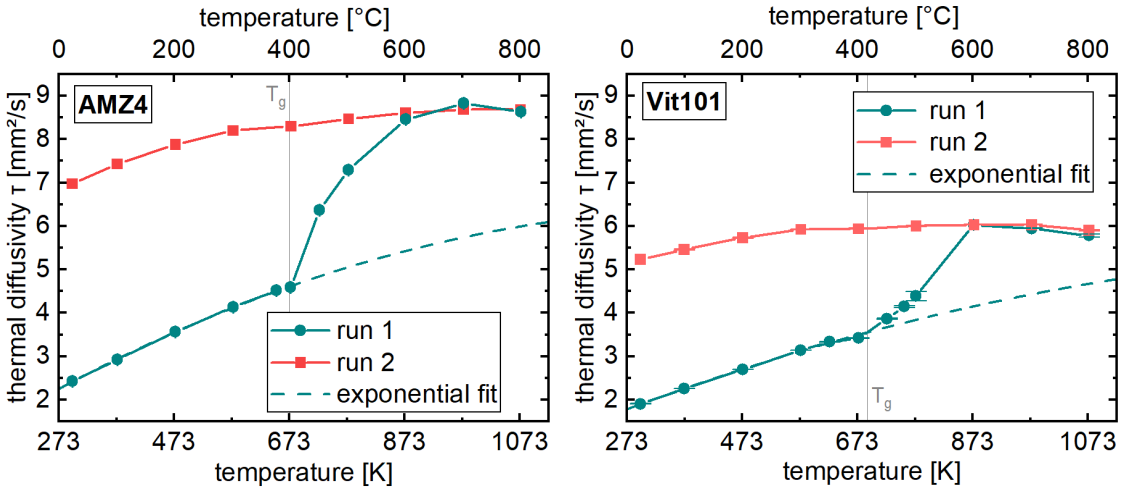

Figure 1: Thermophysical properties: Thermal diffusivity of first and second heating cycle and fit function. Left: AMZ4. Right: Vit101. Acc. to: [40]

In view of the large temperature dependence of the thermal conductivity, an iterative solution of the Rosenthal equation based on temperature-dependent values is motivated. Thus, fit functions are determined for both values. During the measurement by laser flash application, the heating rate caused a crystallization of the samples, This crystallization process differs from the fast heating and cooling rates experienced during PBF-LB/M processing, where such crystallization is not expected to occur. Thus, the progression of the values for the transition of amorphous materials to melt is considered. Based on the measured values for the amorphous materials, the fit function should describe this material behavior. The resulting fit-functions are depicted in Fig. 1 and 2 are given in Tab. 2.

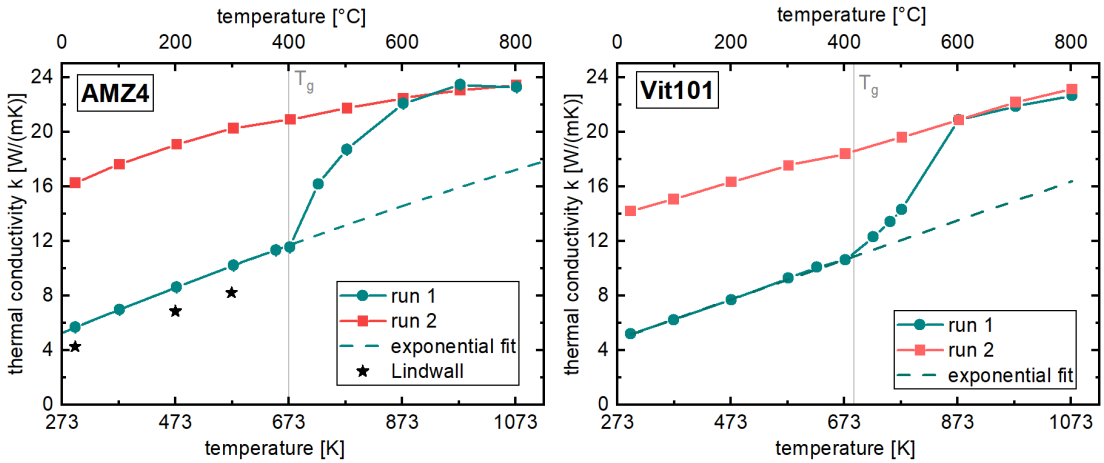

Figure 2: Thermal conductivity in dependence on the temperature, resulting from Laser Flash measurements. Left: AMZ4. Right: Vit101. Acc. to: [40]

Finally, the absorption coefficient is required for the Rosenthal equation. The time-temperature proceeding is obtained by thermocouples during the processing of a 10 mm disc in three consecutive layers. Applying the procedure described above, the effective absorptivity can be averaged to 0.32 for AMZ4 and Vit101. However, it is important to note that the

absorptivity may change based on the processing conditions and applied process parameters [36].

Table 2: Fit functions and absorptivity for AMZ4 and Vit101 used in the following sections.

	AMZ4	Vit101
Th. Diffusivity τ	$10.86446 - 8.43287 * 0.99915^{(T-273.15)}$ mm²/s	$5.86571 - 4.10205 * 0.99867^{(T-273.15)}$ mm²/s
Th. Conductivity k	$50.10777 - 44.81787 * 0.99962^{(T-273.15)}$ W/mK	$372.23529 - 367.44763 * 0.99996^{(T-273.15)}$ W/mK
Absorptivity a	0.32	0.32

Validation of iterative Rosenthal approach

Based on the previously described results for a, k and τ, thermal profiles can be calculated according to eq. 1. However, the conventional Rosenthal model assumes constant thermophysical properties, which hypothetically decreases the prediction accuracy. Fig. 3 exemplarily depicts the x-y isothermal contour plots based on constant thermal diffusivity and thermal conductivity taken at 293 K (LT) and 1073 K (HT). Naturally, the melt pool length and the associated time-Temperature (t-T) curve are elongated assuming the thermophysical properties at room temperature. Under the given conditions, the melt pool length is increased by 19.9 % and the width of the HAZ where T_g is exceeded by 22.4 %.

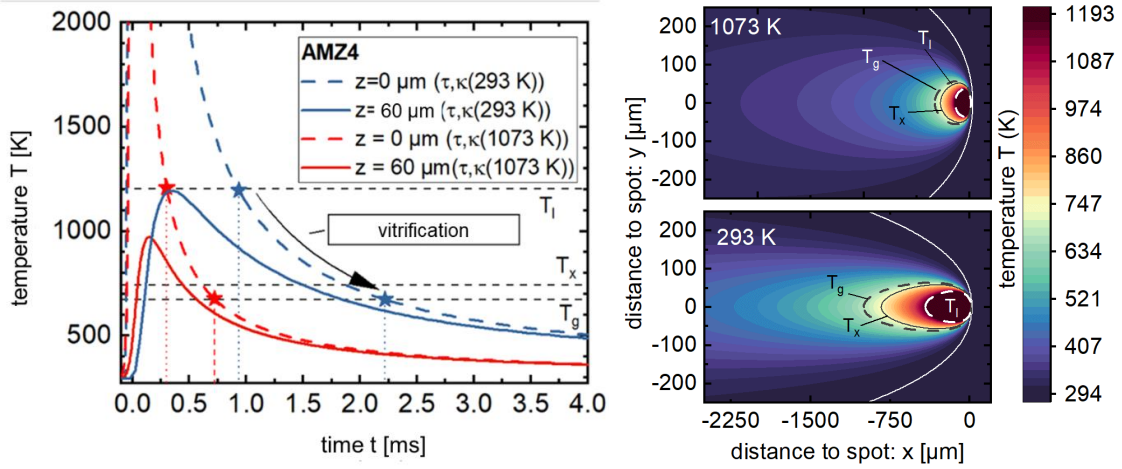

Figure 3: Results of conventional Rosenthal model for AMZ4 with k and τ taken at 293 K and at 1073 K; at P=60 W and v_s=1.4 m/s. Left: T-t diagram for z = 0 µm and z = 60 µm. Right: T-field in the x-y plane. Acc. to [41]

The iterative Rosenthal prediction method is applied to evaluate the influence of T-dependent variables on the prediction of thermal profiles. For this purpose, the determined fit functions for k and τ are inserted into the Rosenthal equation, which then is iterated. During the first iteration step, a high variation of melt pool dimensions occurs. After 5 to 10 iterations, the variation decreases, and after 15 iterations, the values can be assumed to maintain constant.

To validate the iterative Rosenthal prediction, single tracks were processed. The width of the scan track is considered to indicate the width of the isothermal line where the first-order phase transition from liquid to solid takes place – marked in Fig. 3 as T_l. The width of the

processed single tracks based on the applied line energy density is plotted together with the predicted width in Fig. 4 for AMZ4.

It can be seen that the analytically calculated melt pool width correlates to the measured scan track width. To determine the quality of the correlation, Fig. 5 displays the melt pool width in dependence on the energy line density [eq. 5].

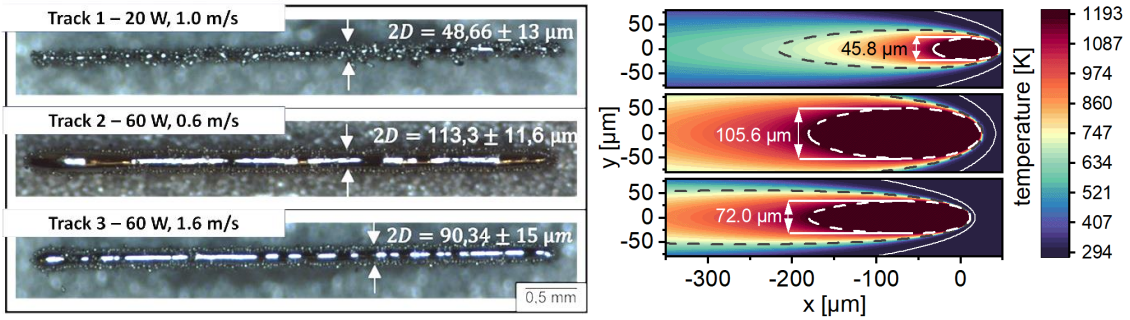

Figure 4: Single tracks of AMZ4. Left: Experimentally determined dimensions. Right: Analytically determined temperature fields. Top: P_L =20 W, v_s =1 m/s. Mid: 60 W, 0.6 m/s. Bottom: 60 W, 1.6 m/s. [41]

For AMZ4 the analytically determined values coincide with the measurement data up to a line energy density of 60 J/m. For higher energy input, a divergence of measured to calculated values can be seen. The basis for the Rosenthal approach is the consideration of conduction and diffusion as the main heat transfer mechanisms. This is assumed to be applicable for low energy input. At higher energy levels, mechanisms of evaporation, convection and keyhole formation can increasingly affect the heat flow and absorption. Thus, the deviation of measured to calculated values at higher E_L can be explained.

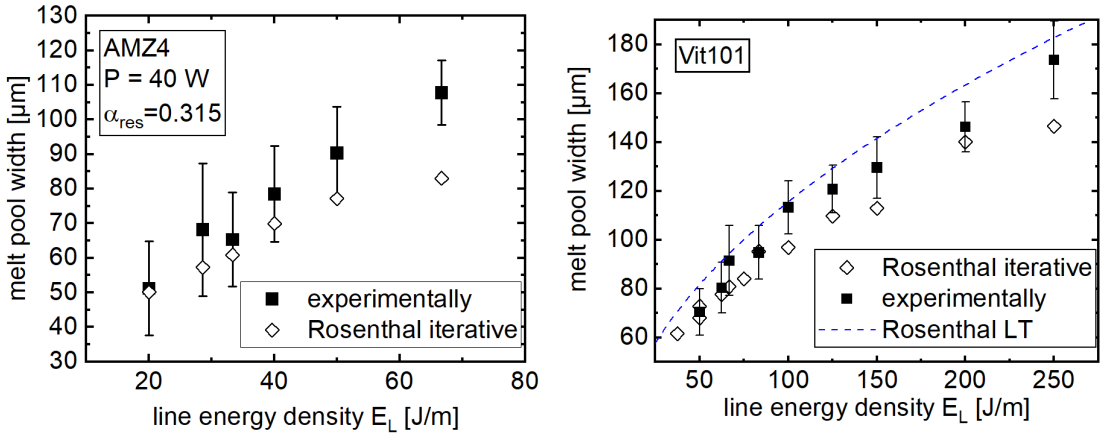

Figure 5: Experimentally and analytically determined scan track width. Left: AMZ4, P_L= const. Right: Vit101, varied P_L and v_s. Acc. to [40]

To evaluate the influence of the process parameters on the thermal cycle, three different manufacturing parameter sets for the glass-forming alloys AMZ4 and Vit101 are examined. The conventional and the iterated approach are applied, and the results compared.

Cooling rates and temperature profiles in single tracks

The iterative Rosenthal approach allows a prediction of temperature fields in the x-y plane, which can be used to estimate the dimensions of the heat-affected zone (HAZ) implying different mechanisms of affection. These are melting, heating above T_g, and heating below T_g. Further, the heating and cooling rates within a single weld track can be calculated, which are meaningful for the vitrification. Fig. 6 (left) shows the t-T diagram for AMZ4 during one heating cycle. As shown in Fig. 6, the cooling time is $t_{c,AMZ4} = 1.3\,ms$ and corresponds to a cooling rate of R = 4·10^5 K/s on the scan path at z = 0. This locates several magnitudes below the nominal critical cooling rate of 5 – 40 K/s for AMZ4 [28]. For Vit101, similar values are achieved.

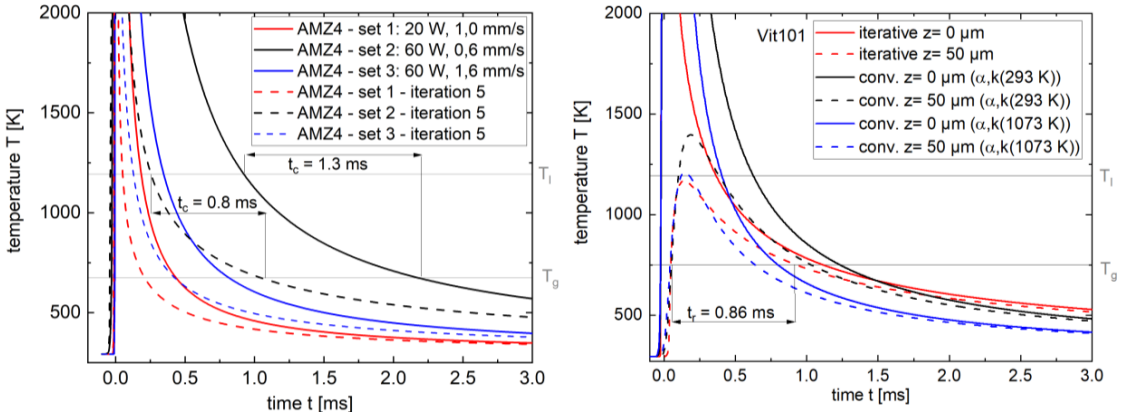

Figure 6: Left: t-T diagram for AMZ4 processed with 3 different parameter sets, comparing conventional and iterated model. Right: t-T diagram for Vit101 processed at 100 W and 0.8 m/s, at z = 0 µm and z = 50µm (lower layer in AM).

To consider the effect of newly applied layers on the underlying material of the produced part, the re-heating of material at different heights of z = 0 µm and z = 50 µm (50 µm below the surface of the melt pool) is calculated and depicted in Fig. 6 (right) for Vit101. The iterated approach presents that at z = 50 µm the material is heated above T_g, but not molten. In this region, the concept of the cooling rate R needs to be adjusted since the entailed t_c describes the cooling from the liquid state to the amorphous state. Instead, here the solid amorphous material is heated to a certain temperature and then cooled again. To describe this, the retention time t_r is introduced as the time a certain point remains in the temperature regime between T_g and T_l:

$$t_r = t_{T\_glass\_transit\_up} - t_{T\_glass\_transit\_down} \qquad \text{Eq. 6}$$

The highest retention time is expected to exceed the highest cooling time and thus $t_{r,max}$ depicts a critical value for the margin of vitrification to partial crystallization. For Vit101 processed at 100W and 0.8 m/s, t_r = 0.86 ms. For a first estimation, concepts concerning critical heating rates and their effect on vitrification issues are neglected here. If t_r is inserted into eq. 3 in place of t_c, it corresponds to a cooling rate of R = 5.56 ·10^5 K/s. This is 5 magnitudes higher than the conservative $R_{crit,Vit101}$ = 62 K/s. Accordingly, successful vitrification can be expected. Crystallization theoretically should not occur within single lines, even in the critical areas of the heat-affected zone.

To discuss the influence of powder instead of solid material surrounding the heat source, the powder bed is approximated as solid with lower conductivity. In this case the thermal

conductivity can be expected to be about two orders of magnitude lower for powder materials compared to solid bulk material [42].

The resulting cooling time according to Fig. 7 at x, y, z = 0 is then t_c = 25 ms, with a resulting cooling rate: R= 520K / 0.025s = 20.8 ·10^3K/s. The critical times of crystallization determined by Yang et al. lie between 14.2 and 22.4 ms for increasing oxygen content [43]. Thus, it can be concluded that at higher layer thicknesses, unsupported areas or downskin regions with an increasing ratio of powder to solid in the direct surroundings of the melt pool in combination with high oxygen contamination of the powder feedstock, crystallization could occur during PBF-LB/M manufacturing of AMZ4. Additionally, consecutive scan tracks within the same layer could affect the cooling times drastically. Due to the complex

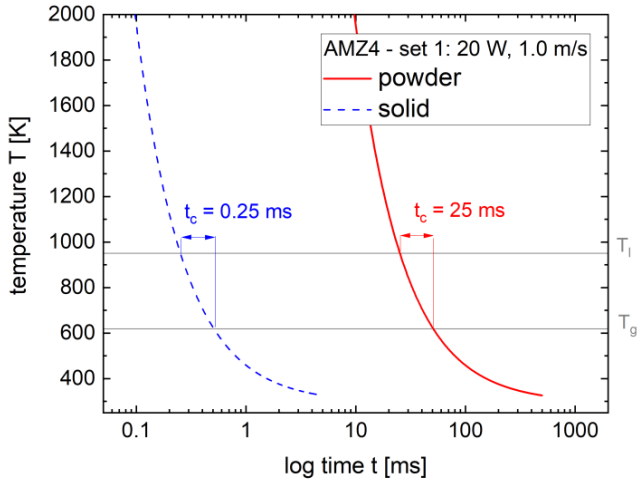

Figure 7: Logarithmic t-T diagram of AMZ4 comparing the proceeding of the temperature for powder and solid material, assuming k = 5.75 for solid material and k = 0.0575 for powder material at 293 K (no iteration).

In theory, for single track manufacturing in PBF-LB/M no crystallization is expected for AMZ4 and Vit101. The calculated cooling rates exceed the critical values by several magnitudes. In practice, partially crystallized samples were detected, which could be correlated to an accumulation of heat by subsequent scan vectors in x-y- or in z-direction (following layers). The pattern and sequence are part of the scan strategy, which can be customized. These findings motivate the consideration of BMGs with lower GFA for PBF-LB/M, such as the novel alloy $Ti_{60}Zr_{15}Cu_{17}S_8$.

Transfer to feasibility of $Ti_{60}Zr_{15}Cu_{17}S_8$

In this section, the Rosenthal equation is applied to estimate the processability of the novel glass-forming alloy $Ti_{60}Zr_{15}Cu_{17}S_8$. Therefore, by Laser Flash measurement of cast material the thermal diffusivity and conductivity are determined in dependence on the temperature, as depicted in Fig. 8 (left). The conductivity shows an almost linear increase with rising temperature. The progression of the diffusivity shows a kink at a temperature of approximately 675 K. In general, the values for the second measurement run are higher than for the first run, which can be correlated to the effect of partial crystallization during the measurement. In order to estimate the general feasibility of vitrification, the t-T progression is calculated once at low temperature (295 K; τ_{LT}=3.55 mm²/s; k_{LT}= 8.76 W/ m· K) and once at

high temperature (1075 K; τ_{HT}= 5.27 mm²/s; k_{HT}= 18.77 W/ m· K). The absorptivity was determined according to eq. 4 using cast material and is a = 0.31 for the chosen process parameters of P= 70 W and v_s= 1.0 m/s. The resulting t-T diagram is given in Fig. 8 (right).

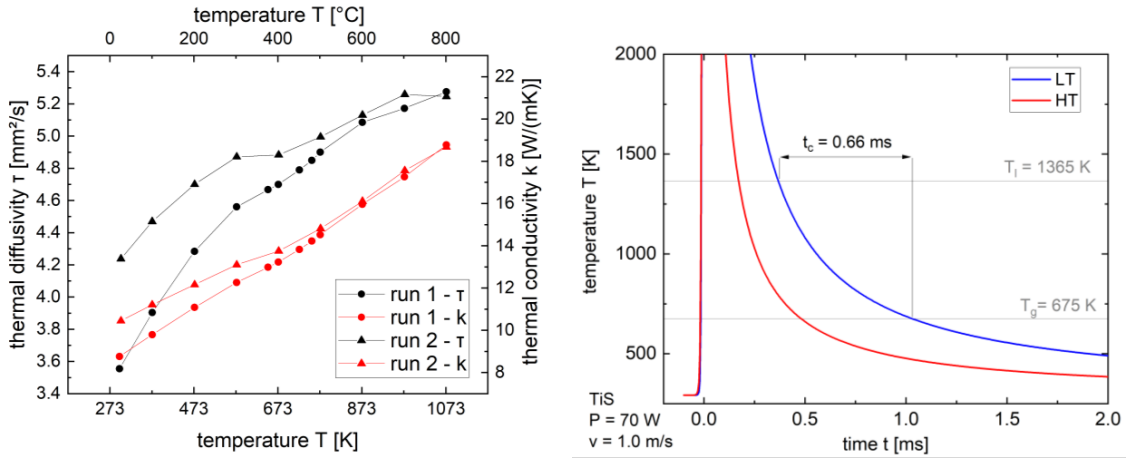

Figure 8: Left: Thermophysical properties τ and k of $Ti_{60}Zr_{15}Cu_{17}S_8$. Right: t-T diagram derived by Rosenthal equation of $Ti_{60}Zr_{15}Cu_{17}S_8$ at low (LT) and high (HT) temperature.

For $Ti_{60}Zr_{15}Cu_{17}S_8$ the cooling time determined by Rosenthal is t_c= 0.66 ms, resulting in a cooling rate of R = 1.0 ·10^6 K/s. For the chosen parameter set, both cooling rates are below the critical cooling rate. The melt pool length is 2 times higher at low temperature. This divergence leads to the assumption that for higher accuracy a fit function could be derived and applied to iterate the Rosenthal equation, as shown above for AMZ4 and Vit101. Nevertheless, this example shows, how the application of temperature-dependent thermal properties to the Rosenthal equation can enable an estimation of vitrification possibilities for novel materials and different processing parameters. Thus $Ti_{60}Zr_{15}Cu_{17}S_8$ can be considered for manufacturing of BMGs via PBF-LB/M.

Conclusion

In this work, the thermophysical properties of AMZ4, Vit101 and Ti60S were measured in dependence on the temperature. For AMZ4 and Vit101, fit functions were determined to describe the thermal conductivity and the thermal diffusivity. The absorption was determined for both materials by in-situ measurement. The resulting values were used to develop an iterative Rosenthal approach, considering the T-dependence of thermal conductivity and diffusivity. The approach was validated for line energy densities below 60 J/m (AMZ4) and 200 J/m (Vit101) and thus can be considered for future analytical applications. Divergence from experimental results is found for higher energy input, which can be explained by an increasing effect of keyhole mode and convection on the heat flow. The approach was then used to estimate cooling rates during the manufacturing by PBF-LB/M of the glass-forming materials AMZ4 and Vit101. The t-T diagrams along the z-height suggest, that the interface between melt pool and heat affected zone is most likely to experience a crystallization, since here the thermal cycle is prolonged. Although the iteratively determined cooling rates exceeded the values according to conventional Rosenthal approach, the nominal R_{krit} is met for all three alloys.

For the novel glass-forming alloy $Ti_{60}Zr_{15}Cu_{17}S_8$, cooling rates and melt pool dimensions were calculated via Rosenthal, considering temperature-dependent thermal conductivity and diffusivity. The resulting cooling times match the allowance. Thus, this

material class is expected to be a promising candidate for BMG processing via PBF-LB/M. The influence of heat accumulation due to subsequent scan tracks and layers needs to be considered in future experiments and simulations to ensure the vitrification on larger scales.

It is reported that single lines of all 3 investigated materials can be processed with cooling rates high enough to enable vitrification. For AMZ4 the limits of processability are highlighted: When heat accumulation (e.g., due to surrounding powder material) occurs combined with higher oxygen contamination of the powder feedstock, the critical cooling times can be exceeded, indicating a risk of partial crystallization.

The results can be summarized as:

1) Within single tracks, successful vitrification is theoretically expected.
2) High cooling rates should enable processing of BMGs with lower GFA.
3) Possible limitations for vitrification: Scan strategy, oxygen contamination in powder feedstock, lack of heat transfer via solid / support.

Outlook

Further optimization steps for increased accuracy of the Rosenthal equation could be performed. It can be suggested to investigate the influence of heat convection on the heat flow, enabling the verified use of an analytical approach to estimate cooling rates and melt pool dimensions at higher energy inputs. Further, material parameters such as T_g, T_x and R_{crit} not only depend on the temperature but also the cooling/heating rates, and therefore a time-dependence could be considered. The quality of raw material also highly affects R_{crit} and could be considered an important factor for quality control as well as for comparison on the side of the limitations of processability.

Additionally, other analytical approaches could be of interest to evaluate and optimize the predictions. Goldak developed an approach based on assuming an elliptical heat source in welding, eliminating the issues concerning point heat sources in the Rosenthal equation [44]. This could be used for likewise simulation, verification, and improvement of existing models.

Acknowledgements

The authors would like to thank Prof. Roland Schmechel from the Institute of Technology for Nanostructures at the University of Duisburg-Essen for their support in carrying out Laser Flash measurements. This research was supported by the German Research Foundation (DFG) through Grant No. KL 3357/1-1. The PBF-LB/M system SLM 280 Hl was funded by the German Research Foundation (DFG) through Grant No. INST 20876/341-1.

References

[1] T. Wohlers, R. I. Campbell, O. Diegel, J. Kowen, N. Mostow, and I. Fidan, *Wohlers report 2022: 3D printing and additive manufacturing : global state of the industry*. Fort Collins, Colo., Washington,DC: Wohlers Associates; ASTM International, 2022.

[2] S. Pauly *et al.,* "Processing metallic glasses by selective laser melting," *Materials Today*, vol. 16, 1-2, pp. 37–41, 2013, doi: 10.1016/j.mattod.2013.01.018.

[3] N. Sohrabi, J. Jhabvala, and R. E. Logé, "Additive Manufacturing of Bulk Metallic Glasses—Process, Challenges and Properties: A Review," *Metals*, vol. 11, no. 8, p. 1279, 2021, doi: 10.3390/met11081279.

[4] C. Suryanarayana and A. INOUE, *Bulk Metallic Glasses, Second Edition,* 2nd ed. Milton: CRC Press, 2017.

[5] M. Telford, "The case for bulk metallic glass," *Materials Today*, vol. 7, no. 3, pp. 36–43, 2004, doi: 10.1016/S1369-7021(04)00124-5.

[6] U. Scipioni Bertoli, G. Guss, S. Wu, M. J. Matthews, and J. M. Schoenung, "In-situ characterization of laser-powder interaction and cooling rates through high-speed imaging of powder bed fusion additive manufacturing," *Materials & Design*, vol. 135, pp. 385–396, 2017, doi: 10.1016/j.matdes.2017.09.044.

[7] J.-H. Jang, H.-G. Kim, H.-J. Kim, and D.-G. Lee, "Crystallization and Hardness Change of the Ti-Based Bulk Metallic Glass Manufactured by a Laser Powder Bed Fusion Process," *Metals*, vol. 11, no. 7, p. 1049, 2021, doi: 10.3390/met11071049.

[8] X. P. Li, C. W. Kang, H. Huang, L. C. Zhang, and T. B. Sercombe, "Selective laser melting of an Al86Ni6Y4.5Co2La1.5 metallic glass: Processing, microstructure evolution and mechanical properties," *Materials Science and Engineering: A*, vol. 606, pp. 370–379, 2014, doi: 10.1016/j.msea.2014.03.097.

[9] H. Liu, Q. Jiang, J. Huo, Y. Zhang, W. Yang, and X. Li, "Crystallization in additive manufacturing of metallic glasses: A review," *Additive Manufacturing*, vol. 36, p. 101568, 2020, doi: 10.1016/j.addma.2020.101568.

[10] X. D. Nong, X. L. Zhou, and Y. X. Ren, "Fabrication and characterization of Fe-based metallic glasses by Selective Laser Melting," *Optics & Laser Technology*, vol. 109, pp. 20–26, 2019, doi: 10.1016/j.optlastec.2018.07.059.

[11] S. V. Madge and A. L. Greer, "Laser additive manufacturing of metallic glasses: issues in vitrification and mechanical properties," *Oxford Open Materials Science*, vol. 1, no. 1, 2020, doi: 10.1093/oxfmat/itab015.

[12] M. Frey *et al.,* "Laser powder bed fusion of Cu-Ti-Zr-Ni bulk metallic glasses in the Vit101 alloy system," *Additive Manufacturing*, vol. 66, p. 103467, 2023, doi: 10.1016/j.addma.2023.103467.

[13] J. Wegner *et al.,* "Influence of powder characteristics on the structural and the mechanical properties of additively manufactured Zr-based bulk metallic glass," *Materials & Design*, vol. 209, no. 3, p. 109976, 2021, doi: 10.1016/j.matdes.2021.109976.

[14] J. Wegner, M. Frey, S. Kleszczynski, R. Busch, and G. Witt, "Influence of process gas during powder bed fusion with laser beam of Zr-based bulk metallic glasses," *Procedia CIRP*, vol. 94, pp. 205–210, 2020, doi: 10.1016/j.procir.2020.09.039.

[15] E. Soares Barreto *et al.,* "Properties of gas-atomized Cu-Ti-based metallic glass powders for additive manufacturing," *Materials & Design*, vol. 215, p. 110519, 2022, doi: 10.1016/j.matdes.2022.110519.

[16] D. ROSENTHAL, "Mathematical Theory of Heat Distribution during Welding and Cutting," *Welding Journal*, vol. 20, pp. 220–234, 1941. [Online]. Available: https://ci.nii.ac.jp/naid/10014566598/

[17] P. Promoppatum, S.-C. Yao, P. C. Pistorius, and A. D. Rollett, “A Comprehensive Comparison of the Analytical and Numerical Prediction of the Thermal History and Solidification Microstructure of Inconel 718 Products Made by Laser Powder-Bed Fusion,” *Engineering*, vol. 3, no. 5, pp. 685–694, 2017, doi: 10.1016/J.ENG.2017.05.023.
[18] S. Imani Shahabad, G. Karimi, and E. Toyserkani, “An Extended Rosenthal’s Model for Laser Powder-Bed Fusion Additive Manufacturing: Energy Auditing of Thermal Boundary Conditions,” *Lasers Manuf. Mater. Process.*, vol. 8, no. 3, pp. 288–311, 2021, doi: 10.1007/s40516-021-00148-0.
[19] J. Liu and A. C. To, “Quantitative texture prediction of epitaxial columnar grains in additive manufacturing using selective laser melting,” *Additive Manufacturing*, vol. 16, pp. 58–64, 2017, doi: 10.1016/j.addma.2017.05.005.
[20] W. E. King *et al.,* “Observation of keyhole-mode laser melting in laser powder-bed fusion additive manufacturing,” *Journal of Materials Processing Technology*, vol. 214, no. 12, pp. 2915–2925, 2014, doi: 10.1016/j.jmatprotec.2014.06.005.
[21] J. J. Marattukalam *et al.,* “Development of process parameters for selective laser melting of a Zr-based bulk metallic glass,” *Additive Manufacturing*, vol. 33, p. 101124, 2020, doi: 10.1016/j.addma.2020.101124.
[22] B. Lane *et al.,* “Transient Laser Energy Absorption, Co-axial Melt Pool Monitoring, and Relationship to Melt Pool Morphology,” *Additive Manufacturing*, vol. 36, 2020, doi: 10.1016/j.addma.2020.101504.
[23] X. H. Lin and W. L. Johnson, “Formation of Ti–Zr–Cu–Ni bulk metallic glasses,” *Journal of Applied Physics*, vol. 78, no. 11, pp. 6514–6519, 1995, doi: 10.1063/1.360537.
[24] A. Kuball, “Development, characterization and processing of a novel family of bulk metallic glasses : sulfur-containing bulk metallic glasses,” Saarländische Universitäts- und Landesbibliothek. [Online]. Available: https://publikationen.sulb.uni-saarland.de/handle/20.500.11880/29345
[25] B. Bochtler, “Thermophysical and structural investigations of a CuTi- and a Zr-based bulk metallic glass, the influence of minor additions, and the relation to thermoplastic forming,” 2019.
[26] J. Heinrich, “Massivglasbildende metallische Legierungen als Konstruktionswerkstoff : Materialoptimierung und Technologieentwicklung zur Herstellung und Verarbeitung,” 2012.
[27] Heraeus Amorphous Alloy Technologies, *Heraeus AMLOY-Zr01 Data Sheet.* [Online]. Available: https://www.heraeus.com/media/media/group/media_group/products/amorphous_metals/datasheets_1/Datasheet_AMLOY-ZR01~2.pdf (accessed: Oct. 3 2021).
[28] I. Jonas, W. Hembree, F. Yang, R. Busch, and A. Meyer, “Industrial grade versus scientific pure: Influence on melt properties,” *Appl. Phys. Lett.*, vol. 112, no. 17, p. 171902, 2018, doi: 10.1063/1.5021764.
[29] I. Hatta, Y. Sasuga, R. Kato, and A. Maesono, “Thermal diffusivity measurement of thin films by means of an ac calorimetric method,” *Review of Scientific Instruments*, vol. 56, no. 8, pp. 1643–1647, 1985, doi: 10.1063/1.1138117.
[30] O. Kubaschewski, C. B. Alcock, and P. J. Spencer, *Materials thermochemistry*. Amsterdam, Boston, Heidelberg: Pergamon Press, 1993.
[31] W. J. Parker, R. J. Jenkins, C. P. Butler, and G. L. Abbott, “Flash Method of Determining Thermal Diffusivity, Heat Capacity, and Thermal Conductivity,” *Journal of Applied Physics*, vol. 32, no. 9, pp. 1679–1684, 1961, doi: 10.1063/1.1728417.
[32] J. A. Cape and G. W. Lehman, “Temperature and Finite Pulse-Time Effects in the Flash Method for Measuring Thermal Diffusivity,” *Journal of Applied Physics*, vol. 34, no. 7, pp. 1909–1913, 1963, doi: 10.1063/1.1729711.

[33] W. E. King *et al.,* “Laser powder bed fusion additive manufacturing of metals; physics, computational, and materials challenges,” *Applied Physics Reviews*, vol. 2, no. 4, p. 41304, 2015, doi: 10.1063/1.4937809.
[34] E. Hagen and H. Rubens, “Über Beziehungen des Reflexions- und Emissionsvermögens der Metalle zu ihrem elektrischen Leitvermögen,” *Ann. Phys.*, vol. 316, no. 8, pp. 873–901, 1903, doi: 10.1002/andp.19033160811.
[35] M. Matthews, J. Trapp, G. Guss, and A. Rubenchik, “Direct measurements of laser absorptivity during metal melt pool formation associated with powder bed fusion additive manufacturing processes,” *Journal of Laser Applications*, vol. 30, no. 3, p. 32302, 2018, doi: 10.2351/1.5040636.
[36] N. Schnell, J. Wegner, A. Elspaß, and S. Kleszczynski, “Effective absorptivity of diamond-reinforced metal matrix composites for powder bed fusion using a laser beam,” *Additive Manufacturing Letters*, vol. 6, p. 100138, 2023, doi: 10.1016/j.addlet.2023.100138.
[37] W. Meiners, *Direktes selektives Laser Sintern einkomponentiger metallischer Werkstoffe*. RWTH Aachen, Dissertation, 1999. Aachen: Shaker, 1999.
[38] J. Lindwall, “Modelling of Bulk Metallic Glass formation in Powder Bed Fusion,” Luleå University of Technology, 2019. [Online]. Available: https://www.diva-portal.org/smash/record.jsf?pid=diva2:1283720
[39] M. Yamasaki, S. Kagao, and Y. Kawamura, “Thermal diffusivity and conductivity of Zr55Al10Ni5Cu30 bulk metallic glass,” *Scripta Materialia*, vol. 53, no. 1, pp. 63–67, 2005, doi: 10.1016/j.scriptamat.2005.03.021.
[40] Jan Wegner, “Funktionalisierung der prozessinhärenten Abkühlraten des Laser-Strahlschmelzens zur Verarbeitung metallischer Massivgläser,” Universität Duisburg-Essen, Duisburg, tbp.
[41] Jan Wegner, *Funktionalisierung der prozessinhärenten Abkühlraten des Laser-Strahlschmelzens zur Verarbeitung metallischer Massivgläser*. Dissertationsschrift.
[42] M. R. Alkahari, T. Furumoto, T. Ueda, A. Hosokawa, R. Tanaka, and M. S. Abdul Aziz, “Thermal Conductivity of Metal Powder and Consolidated Material Fabricated via Selective Laser Melting,” *KEM*, 523-524, pp. 244–249, 2012, doi: 10.4028/www.scientific.net/KEM.523-524.244.
[43] Z. Yang, R. Al-Mukadam, M. Stolpe, M. Markl, J. Deubener, and C. Körner, “Isothermal crystallization kinetics of an industrial-grade Zr-based bulk metallic glass,” *Journal of Non-Crystalline Solids*, vol. 573, no. 9, p. 121145, 2021, doi: 10.1016/j.jnoncrysol.2021.121145.
[44] J. Goldak, A. Chakravarti, and M. Bibby, “A new finite element model for welding heat sources,” *Metall Mater Trans B*, vol. 15, no. 2, pp. 299–305, 1984, doi: 10.1007/BF02667333.

Appendix

Table A-1: Machine and material data

Data for PBF-LB/M	Vit101	AMZ4
Machine Spot size P_L	SLM 280 80 µm <700 W	Eos M100 40 µm <200 W
layer thickness hatch	20 µm 90 µm	20 µm
powder	Argon atomized 20-63 µm particle size	Produced by Heraeus

Table A-2: Overview on depicted processing parameters chosen for calculations and manufacturing of single tracks

Set	**Processing Parameters**	**AMZ4**	**Vit101**	$\mathbf{Ti_{60}Zr_{15}Cu_{17}S_8}$
1	v_s	1.0 m/s	0.8 m/s	1.0 m/s
	P_L	20 W	100 W	70W
	Layer thickness	20 µm	20 µm	
2	v_s	0.6 m/s		
	P_L	60 W		
	Layer thickness	20 µm		
3	v_s	1.6 m/s		
	P_L	60 W		
	Layer thickness	20 µm		